

Particle Velocity Distributions and Ionization Processes in a Gas-Puff Z Pinch

M. E. Foord,* Y. Maron, G. Davara, L. Gregorian, and A. Fisher†

Department of Physics, Weizmann Institute of Science, Rehovot, 76100, Israel

(Received 21 December 1993)

We have measured the time-dependent radial velocity distributions of singly to five times ionized ions in an imploding plasma shell by observing the spectral shapes and intensities of emission lines in various directions. An ionization wave propagating much faster than the local radial ion velocities is observed. The ionization front velocity is found to be consistent with estimates of electron heat conduction into the plasma-neutral layer. The ionization and velocity histories of the particles are experimentally determined. The mechanisms of momentum transfer to the particles are also determined and compared with existing models.

PACS numbers: 52.55.Ez, 52.70.Kz

Much effort is presently directed towards understanding dynamic processes in pinches, especially the radiation dynamics in plasma with ions of medium to high nuclear charge [1]. These experiments are beginning to provide insight into the behavior and properties of the final hot dense state of the Z-pinch plasma as well as provide unique opportunities for testing theoretical predictions such as radiative collapse [2]. Other interest in pinch phenomena includes x-ray laser schemes and source development [1], as well as in solar flare plasma, where time-dependent processes are studied [3].

However, the complicated interactions that occur in the initial or implosion phase of the Z-pinch plasma are not well understood as yet. Few studies have focused on the implosion dynamics, despite the numerous studies that have led to much understanding of the final pinch plasma. In the Z-pinch configuration, the axially driven current interacts with its self-induced magnetic field, accelerating the particles radially inward. When the particles reach the central axis, their directed energy thermalizes, forming a hot dense plasma. Thus, the conditions of the final state are determined, to a large extent, during this important initial period when the particles are accelerated and ionized. In this Letter we investigate in detail the particle dynamics and ionization phenomena in an imploding plasma using line emission from the accelerating particles. Measurements of the charge-state and radial velocity distributions are used to develop a model for the ionization processes and particle flows in the pinch and to determine the dominate mechanism of momentum transfer to the particles.

Earlier studies indicated that radial electric fields may play an important role in the implosion dynamics in pinches [4]. In a gas-puff Z-pinch experiment, Bailey *et al.* [5] showed that an initial mixture of heavy and light particles separated into distinct annular regions during the implosion. A two fluid model was later proposed by Barak and Rostoker [6], suggesting that a quasistatic radial electric field generated by the electron pressure gradient was responsible. However, as described below,

we find that the contribution to the accelerating force on ions from the electron pressure gradient is relatively small. A strong local electric field would also tend to accelerate highly charged ions to the front of the shell, which is inconsistent with the presently observed charge-state distributions. We also observe that the radial velocity and charge-state distributions vary gradually across the shell radius throughout most of the implosion. These results thus appear inconsistent with standard snowplow or fully developed shock-wave models that predict strong gradients in pressure and velocity [7, 8].

The Z-pinch experiment and the optical arrangement are shown in Fig. 1. The plasma is formed by first injecting a gas shell ($R \approx 2$ cm, $\delta r \approx 5$ mm) through an annular nozzle into the vacuum region between the anode and cathode that are separated axially by 14 mm. A 290 kA current rising in $1.2 \mu\text{s}$ produces a pinch at $t \approx 600$ ns, as indicated by a strong dip in the B_θ -probe trace at that time. The anode consists of a 4 cm inner diam tube, and the gas used in these experiments was CO_2 .

The main diagnostic employed was a 1.3 m spectrograph coupled to a high-resolution streak camera; see Fig. 1. This system has good sensitivity between 2000

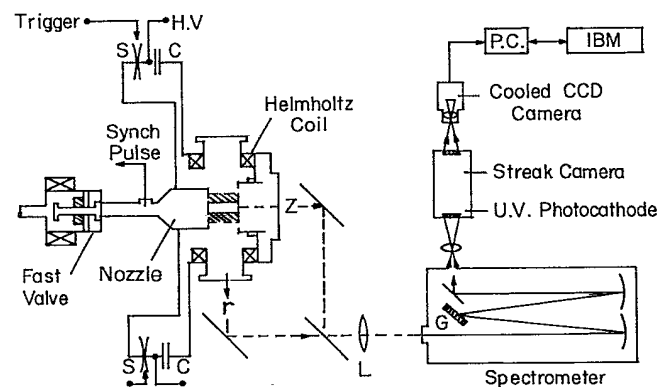


FIG. 1. The Z-pinch experiment and the optical arrangement of the spectrometer and streak camera detector system.

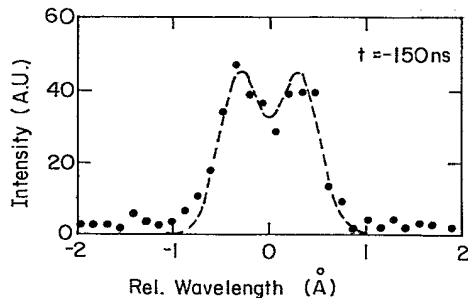


FIG. 2. A typical O III line profile ($\lambda_0 = 3047.1 \text{ \AA}$) measured radially at $z = 11 \text{ mm}$ and $t' = -150 \text{ ns}$. Redshifted and blueshifted components from each side of the annulus are observed. Doppler shifts correspond to a radial velocity $\approx 3 \text{ cm}/\mu\text{s}$.

and 8000 \AA , and allows time-dependent spectral line shapes and intensities to be obtained in a single discharge. The instrumental spectral and temporal resolutions are 0.04 \AA and 100 ps , respectively. The input optics provides typically $\approx 0.5 \text{ mm}$ horizontal and 2.0 mm vertical resolutions in the plasma. The streak camera output is imaged by a cooled charge-coupled device camera, providing linear response over the dynamic range of the instrument.

Spectra were obtained in the radial direction along chords normal to the central axis at various distances z from the cathode. Shown in Fig. 2 is a typical profile of the O III 3047.1 \AA line observed in the radial direction at $z = 11 \text{ mm}$ and $t' = -150 \text{ ns}$. Here, t' is with respect to the pinch time. The data are fit by two shifted Gaussian distributions. All line shapes used here were checked to be dominated by Doppler effects during the time period addressed in this study. The average radial velocity of the particles is determined from $v_r = c\Delta\lambda_s/2\lambda$, where $\Delta\lambda_s$ is the spectral distance between the Doppler shifted distributions. As presented below, axial measurements indicate that the various charge states are distributed in thin shells of a few millimeters thickness. Therefore, Fig. 2 represents the localized radial velocity distribution of the O III ions moving radially inward from each side of the shell.

The radial velocity of O III–O VI ions is shown in Fig. 3. The velocities are obtained from the O III 3047.1 \AA ($2p3s^3P^o-2p3p^3P$), O IV 3063.5 \AA ($2s^23s^2S-2s^23p^2P^o$), O V 2781.0 \AA ($2s3s^3S-2s3p^3P^o$), and O VI 3811.4 \AA ($3s^2S-3p^2P^o$) lines. The velocities of each charge state ion are seen to increase with charge, reaching $10 \text{ cm}/\mu\text{s}$ in the case of O VI. The velocity distributions of O II ions (not shown) were determined from the 4349.4 \AA ($2p^23s^4P-2p^23p^4P^o$) transition and are best fit by a single Gaussian, indicating a radial velocity $\leq 1 \text{ cm}/\mu\text{s}$.

Line-intensity radial distributions are obtained from axial measurements taken along various chords parallel to the z axis. Emission from O II and O III transitions is

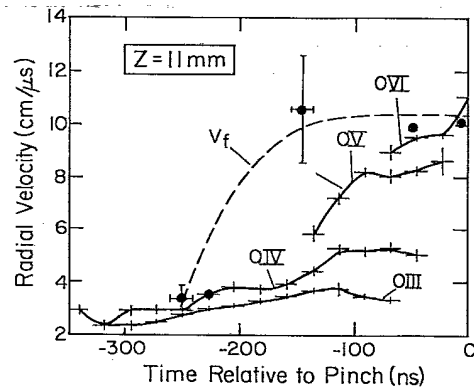


FIG. 3. The radial velocity of O III–O VI ions. Each curve is averaged over 3–5 similar discharges and the error bars represent the shot-to-shot variation. The ionization wave front velocity V_f , determined from axial measurements of the O II cloud velocity, is shown for comparison.

first observed near the initial radius of $r = 2 \text{ cm}$. At later times, as shown in Fig. 4, higher charge states appear at the outer edge of the shell. The motion of ion clouds is determined from the axial measurements of the maximum intensity taken at 1–2 mm radial intervals. The O II cloud reaches a velocity near $10 \text{ cm}/\mu\text{s}$ at $t' = -100 \text{ ns}$; see Fig. 3.

An important finding is that the observed motion of the charge-state clouds is much faster than the Doppler velocities, particularly in the case of O II as mentioned above. In addition, higher charge states are observed at larger radii than the lower charge states, leading us to suggest that the fast motion of the charge-state clouds is due to an ionization wave that propagates at the leading edge of the plasma annulus. Note that since the higher-charge-state ions move at a velocity similar to the ionization wave front, the total thickness of the shell remains nearly constant up to $t' \approx -40 \text{ ns}$.

We now consider the possibility that the ionization wave is driven by electron heat conduction from the hotter outside edge. Detailed modeling would require an accurate accounting for the electron cooling and heating processes as well as heat transport through the plasma. Here, we balance the thermal flux into the O II region of the

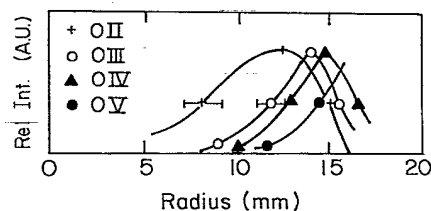


FIG. 4. Line-intensity radial distributions for O II–O V ions at $t' = -110 \text{ ns}$. For comparison, each line is normalized to its peak intensity. Based on collisional radiative calculations these distributions reflect the total ion density distributions [10].

ionization wave due to electron heat conduction with the energy required to ionize the incoming flux of neutrals, i.e.,

$$V_f \left(n_0 I_0 + \frac{5}{2} n_e T_e \right) = \kappa_e \frac{dT_e}{dr}. \quad (1)$$

Here, V_f is the velocity of the ionization front, n_0 is the neutral CO_2 density, I_0 is the dissociation plus ionization energy per molecule (53.1 eV to produce O II and C II), and κ_e is the effective electron heat conductivity coefficient [9].

Based on comparisons of oxygen line-intensity ratios [10] with collisional radiative model calculations (similar calculations can be found in [11–13]) we estimate the electron temperature between the O II and O III clouds to be ≈ 8 eV at times between $t' = -100$ and -50 ns, when the ionization wave front traverses the region $r = 10$ to 5 mm. The O II cloud thickness is ≈ 0.2 cm and $\bar{n}_0 \approx 5 \times 10^{15}$, as estimated from gas probe measurements averaged over this region. The gas profile was determined from a calibrated miniature Penning probe placed at various positions with respect to the nozzle, as described in detail in Ref. [14]. Using these parameters we obtain $V_f = 5 \times 10^6$ cm/s. While this estimate is strongly dependent on $T_e(r)$ (through the T_e dependence of κ), this estimate is in reasonable agreement with the $\approx 10^7$ cm/s value observed for this time period. This discussion assumes no electron joule heating at the plasma-neutral layer interface, which is the subject of a future research. Photoionization was also considered as a cause of the neutral particle ionization; however, its effect is estimated to be small.

The measurements described above support the general picture of particles being first ionized on the inner edge of the annulus and then further ionized and accelerated as the plasma sweeps over them, eventually reaching the highest charge state and velocity at the outer radius of the plasma. The combination of the radial velocity measurements for each charge-state ion and the axial observations that give the time-dependent radial velocities of each charge-state ion cloud allows us to determine the velocity at each radius. This information is represented as velocity contours in Fig. 5. Near $t' = -170$ ns the O II cloud is seen to expand inward due to the ionization wave, broadening the plasma shell. Later, near $t' = -70$ ns, the outer edge "catches up," steepening the velocity gradient and apparently forming a shocklike structure.

The velocity contours are also used to determine the ion velocity history of any group of ions. The radial position of a group of particles is given by $r(t) = \int v(r(t)) dt$. The trajectory is calculated at 10 ns increments for an initial group of particles starting as O II at $t' = -170$ ns and $r = 16.5$ mm (see Fig. 5) and ending at higher charge state O V. After ≈ 40 ns, the initial O II particles have ionized into O III. Subsequently, these particles ionize into O IV and O V after times 30 and 25 ns, respectively. This method allows a direct determination of the ionization times for this group of particles as they move up the velocity gradient to the outer radius of the shell.

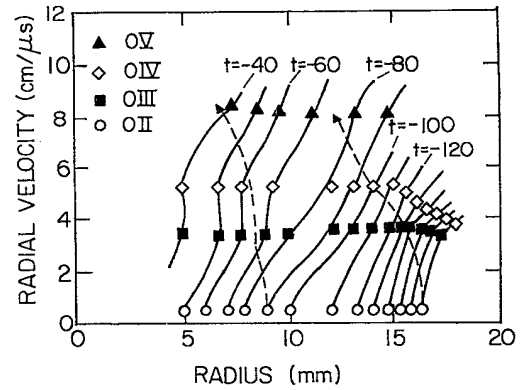


FIG. 5. Particle velocity contours between $t' = -170$ and -40 ns. The calculated trajectories of two groups of particles initially located at $r = 16.5$ and 9 mm are also shown, indicating the velocity histories and ionization times for the various charge states.

Knowledge of the dominant forces that act on the ions requires an experimental determination of the magnetic field distribution in the plasma, which is a subject of our current work. The degree of field penetration in gas-puff Z-pinch devices is currently not known. Here we write the momentum transfer to the ions for the simple case of no magnetic field penetration. In this case, the 1D momentum equation for the above group of particles (identified by subscript α) is given by [15]

$$\frac{\partial}{\partial t} (Mn_\alpha V_{\alpha r}) + \frac{\partial}{\partial t} (Mn_\alpha \langle v_{\alpha r}^2 \rangle) - eZ_\alpha n_\alpha E_r = R_{\alpha i} + R_{\alpha e}. \quad (2)$$

Here, n_α is the total ionic charge ($n_\alpha = \sum n_i$), V_α is the average local velocity of the ions ($V_\alpha \equiv \sum n_i V_i / \sum n_i$), $\langle v_{\alpha r}^2 \rangle$ is the squared radial velocity, averaged over the velocity distribution of the initial group of particles α , and Z_α is the average local charge in the plasma ($Z_\alpha \equiv \sum Z_i n_i / \sum n_i$). The momentum gained by the particles is due to the electric field E_r and due to collisions with electrons ($R_{\alpha e}$) and other ions ($R_{\alpha i}$). Ohm's law is then written as

$$en_e E_r + R_{e\alpha} = -\nabla p_e,$$

where the second term accounts for the electron collisions with ions. We first eliminate $R_{\alpha i}$ in Eq. (2) by combining Eq. (2) with Ohm's law, using $Z_\alpha n_\alpha \equiv n_e$ and $R_{e\alpha} + R_{\alpha e} = 0$. Integrating Eq. (2) over the radial dimension eliminates the second term due to the fact that the density of the group of particles we are following, n_α , is zero at its boundaries. Further integrating in time between t_1 and t_2 yields

$$\int Mn_\alpha V_{\alpha r} dr \Big|_{t_2} = \int_{t_1}^{t_2} dt \int (R_{\alpha i} - \nabla p_e) dr. \quad (3)$$

The data presented in Fig. 5 allow us to estimate the relative contributions to the radial force exerted on

this group of particles as they move to the outside radius $r = 13.8$ mm at $t_2 = -75$ ns (see Fig. 5), using the following simple approximations. The momentum gain at t_2 is approximated as $Mn_\alpha \delta r_\alpha V_{ar}(t_2)$, where $n_\alpha \delta r_\alpha$ is the constant areal density of the particles. This term is compared to the electron pressure gradient force that we assume constant during this period and approximated as $T_{eo} Z_0 n_\alpha \delta r_\alpha \Delta t / \Delta r$, where $\Delta t = t_2 - t_1$, Δr is the width of the shell during this time, Z_0 and T_{eo} are the average charge-state and electron temperature at the outer edge ($Z_0 \approx 3.5$ and $T_{eo} \approx 30$ eV), and $\Delta r / \Delta t \approx V_f \approx 10^7$ cm/s. Comparing these terms, we find that the total momentum gained by the ions is approximately 10 times larger than the ∇p_e contribution.

Assuming little or no magnetic field penetration, it appears that the following situation occurs: At the plasma edge the $\mathbf{j} \times \mathbf{B}$ electric field accelerates ions inward. Their momentum is then continuously transferred to other ions in the plasma via collisions. The other possible source of ion acceleration in the inner part of the plasma, ∇p_e , appears to contribute little in transmitting the momentum to the ions in the plasma.

If the magnetic field is assumed to penetrate, ions gain momentum from a combination of the $\mathbf{j} \times \mathbf{B}$ force and collisions. In this case the relative contribution of the $\mathbf{j} \times \mathbf{B}$ force becomes important for low densities. However, the relative contribution from the ∇p_e force remains small because of the density dependence of the ∇p_e term.

It is interesting to compare these results to the model of Barak and Rostoker [6] who also assumed no magnetic field penetration. However, in their model ions are accelerated solely by the ∇p_e force as they encounter a shock wave, while the momentum gained from ion collisions is assumed negligible. Note that, in our present experiment, the ions are highly collisional (the estimated collision time and mean free path are ≈ 1 ns and ≈ 0.1 mm, respectively), and the electric field generated by the electron pressure gradient is too low to accelerate the ions.

In conclusion, we have observed the propagation of an ionization wave and have shown that inward radial heat conduction is sufficient to support the ionization propagation. An important distinction of these results from those in previous models is that we find no shock front in which all ionization states are present and are accelerated. Such a shock front could also lead to the higher-charge-state ions accelerating ahead (as in [6]), which is inconsistent with the results presented above. In our situation, where the ions are not accelerated in the ionization wave front and if the magnetic field does not penetrate the plasma, particles gain their momentum via collisions with the fast ions at the outside edge. The higher charge states then have higher velocities because they spend a longer time in the plasma and have more time to collide. Thus, it is the relatively low ionization

rates that make the higher charge states flow behind the lower charge states, even though they acquire higher velocities.

Future work will include investigating the magnetic field distribution in the plasma and detailed hydrodynamic calculations to better understand these results. These methods and results should also be relevant to the study of the dynamics of medium- to high-Z material pinches that are also composed of various distributions of multiple-charge-state ions.

The authors are indebted to A. Fruchtman for his valuable theoretical support and to J. Shiloh for his help with the design of the experiment and diagnostic systems. We are also grateful to R. Lovberg, J. Davis, Z. Zinamon, A. E. Blaugrund, N. Rostoker, L. I. Rudakov, K. Matzen, and I. Lindemuth for helpful discussions. We thank P. Meiri and Y. Danino for their technical support. This work was performed under the support of Minerva Foundation, Munich, Germany. M. E. F. acknowledges support in part from Lawrence Livermore National Laboratory, DOE Contract No. W-7405-Eng-48.

*Present address: University of California, Lawrence Livermore National Laboratory, Livermore, CA 94550.

†Present address: Naval Research Laboratory, Washington, D.C. 20375.

- [1] See, for example, *Dense Z-Pinches*, edited by N. R. Pereira, J. Davis, and N. Rostoker, AIP Conf. Proc. No. 195 (American Institute of Physics, New York, 1989).
- [2] V. V. Vikhrev, *Sov. J. Plasma Phys.* **8**, 688 (1982).
- [3] J. M. Laming and U. Feldman, *Astrophys. J.* **386**, 364 (1991).
- [4] R. J. Comisso and H. J. Kunze, *Phys. Fluids* **18**, 392 (1975).
- [5] J. Bailey, Y. Ettinger, A. Fisher, and N. Rostoker, *Appl. Phys. Lett.* **40**, 460 (1981).
- [6] G. Barak and N. Rostoker, *Appl. Phys. Lett.* **41**, 918 (1982).
- [7] M. Rosenbluth, R. Garwin, and A. Rosenbluth, Los Alamos Scientific Laboratory Report No. LA-1850, 1954 (unpublished).
- [8] T. Miyamoto, *Nucl. Fusion* **24**, 337 (1984).
- [9] L. Spitzer, *Physics of Fully Ionized Gases* (Interscience, New York, 1962).
- [10] G. Davara, L. Gregorian, E. Kroupp, and Y. Maron (to be published).
- [11] M. E. Foord, Y. Maron, and E. Sarid, *J. Appl. Phys.* **68**, 5016 (1990).
- [12] M. E. Foord and E. Nardi, *J. Appl. Phys.* **69**, 5028 (1990).
- [13] Y. Maron, M. Sarfaty, L. Perelmutter, O. Zahavi, M. E. Foord, and E. Sarid, *Phys. Rev. A* **40**, 3240 (1989).
- [14] L. Gregorian, M.Sc. thesis, Feinberg Graduate School, Weizmann Institute of Science, 1993.
- [15] S. I. Braginskii, in *Review of Plasma Physics*, edited by M. A. Leontovich (Consultants Bureau, New York, 1965), Vol. 1, p. 205.